

This is the accepted manuscript version of the contribution published as:

Gharasoo, M., Elsner, M., van Cappellen, P., **Thullner, M.** (2022):
Pore-scale heterogeneities improve the degradation of a self-inhibiting substrate: Insights from reactive transport modeling
Environ. Sci. Technol. **56** (18), 13008 - 13018

The publisher's version is available at:

<http://doi.org/10.1021/acs.est.2c01433>

Pore-scale heterogeneities improve the degradation of a self-inhibiting substrate: Insights from reactive transport modeling

Mehdi Gharasoo^{1,2,4,*}, Martin Elsner³, Philippe Van Cappellen⁴, and Martin Thullner^{1,5,*}

¹Helmholtz Centre for Environmental Research - UFZ, Department of Environmental Microbiology, Permoserstr. 15, 04318 Leipzig, Germany

²Bundesanstalt für Gewässerkunde, Abteilung Quantitative Gewässerkunde, Am Mainzer Tor 1, 56068 Koblenz, Germany

³Technical University of Munich, Chair of Analytical Chemistry and Water Chemistry, Marchioninstr. 17, 81377 Munich, Germany

⁴University of Waterloo, Department of Earth and Environmental Sciences, Ecohydrology Research Group, 200 University Av W, Waterloo, ON N2L3G1, Canada

⁵Federal Institute for Geosciences and Natural Resources (BGR), Hannover, Germany

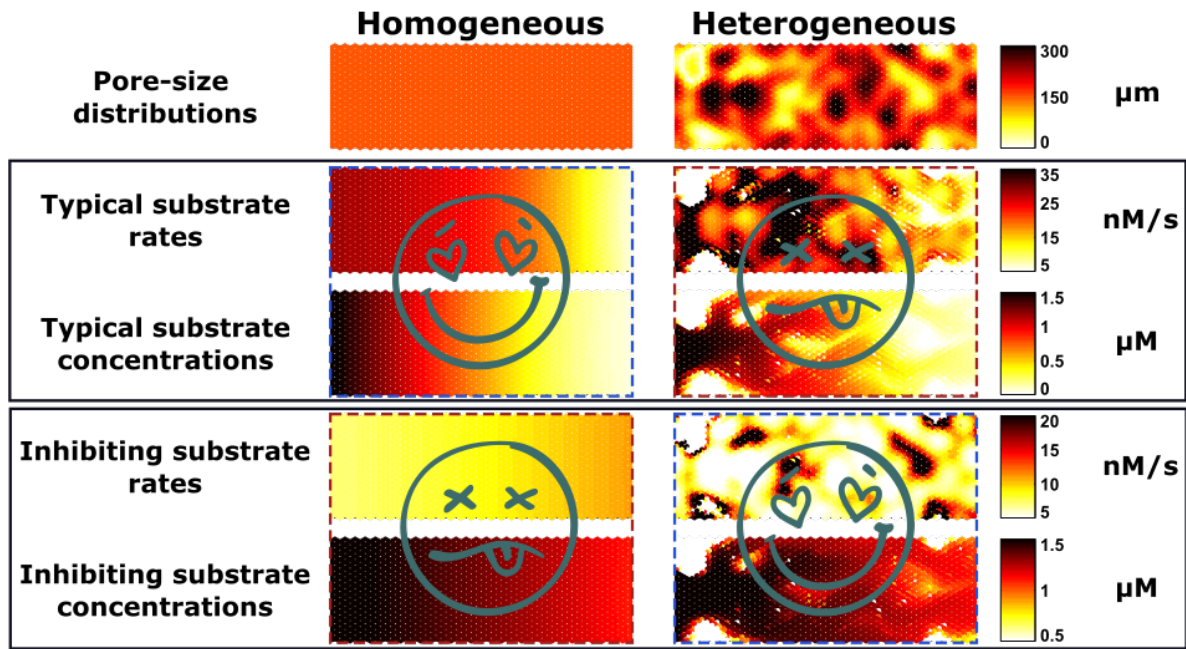
*Corresponding authors: Tel. +49 511 643-3077 , E-mail: martin.thullner@bgr.de, mehdi.gharasoo@ufz.de

Abstract

In-situ bioremediation is a common remediation strategy for many groundwater contaminants. It was traditionally believed that (in the absence of mixing-limitations) a better in-situ bioremediation is obtained in a more homogeneous medium where the even distribution of both substrate and bacteria facilitates the access of a larger portion of bacterial community to a higher amount of substrate. Such conclusions were driven with the typical assumption of disregarding substrate inhibitory effects on the metabolic activity of enzymes at high concentration levels. To investigate the influence of pore matrix heterogeneities on substrate inhibition, we use a numerical approach to solve reactive transport processes in the presence of pore-scale heterogeneities. To this end, a rigorous reactive pore network model is developed and used to model reactive transport of a self-inhibiting substrate at both transient and steady state conditions through media with various, spatially correlated, pore-size distributions. For the first time, we explore on the basis of a pore-scale model approach the link between pore-size heterogeneities and substrate inhibition. Our results show that for a self-inhibiting substrate (1) pore-scale heterogeneities can consistently promote degradation rates at toxic levels, (2) the effect reverses when the concentrations fall to levels essential for microbial growth, and (3) an engineered combination of homogeneous and heterogeneous media can increase the overall efficiency of bioremediation.

Synopsis: Pore-size heterogeneities of subsurface environments help indigenous microorganisms better degrade toxic organic compounds.

Keywords: *Pore-scale Heterogeneities; Contaminant Biodegradation; Substrate Self-inhibition; Pore Network Modeling; Bioavailability*



TOC Art

1 Introduction

Biodegradation of contaminants inside porous media like soils or aquifers is effective as long as the concentrations of biodegradable contaminant is not higher than a certain level triggering inhibitory effects on microbial degraders. At relatively high concentrations, organic substances can impose an adverse effect on degradation rates of catabolic enzymes. The mechanism is known as substrate self-inhibition and regarded as a limiting process in bioremediation of contaminants in subsurface environments^{1,2}. Substrate inhibition has been both experimentally and theoretically investigated and a vast number of contaminants at high concentration levels are shown to be toxic to the microorganisms metabolizing them³⁻⁶. Bioavailability effects on the other hand determine how much of a contaminant is accessible to bacteria. Hence, natural attenuation of contaminants inside porous environments such as soils and aquifers is effective as long as their bioavailability is guaranteed and their concentration is lower than inhibitory levels toxic for microorganisms. At certain conditions, the interplay between the two processes (substrate self-inhibition and its bioavailability) can improve the biodegradation efficiency and enhance the bacterial growth⁷. Whereas outside these conditions, it either results in extreme famine or causes microorganisms to develop a defensive mechanism against substrate toxicity, both leading to the further decay of degradation rates^{5,8}.

Natural porous environments such as soils and aquifers are characterized by various pore-scale

19 heterogeneities that are often considered as another rate-limiting factor for in-situ biodegrada-
20 tion. The heterogeneities form as the result of overlapping sequences of sedimentary struc-
21 tures possessing dissimilar transport properties such as permeability and porosity. Such hetero-
22 geneities as indigenous characteristics of sedimentary basins play an important role in controlling
23 the distribution of contaminants inside the porous media⁹⁻¹¹, the mixing between contaminant
24 and their reaction partners¹²⁻¹⁵, the formation of preferential flow paths¹⁶⁻¹⁸, the temporal
25 variability of substrate supply¹⁹⁻²¹, the resilience of microbial ecosystems subjected to distur-
26 bances²², and the spatial distribution of microorganisms²³⁻²⁵. As a consequence, optimum
27 microbial degradation potential in a natural porous medium may differ from typical laboratory
28 setups for studying microbial behavior²⁶. The presence of pore-scale heterogeneities in natural
29 environments often cause the formation of preferential flow paths that leads to complex dis-
30 tribution patterns of both substrate and bacteria. This obstructs the even distribution of the
31 substrate inside the media, increases the occurrence of stress periods on microbial population,
32 and reduces the substrate accessibility to indigenous microorganisms²⁷. The adverse effect of
33 medium heterogeneity on degradation of a substrate was shown both experimentally and the-
34 oretically²⁸⁻³⁰ unless a mixing effect with another reactant (e.g. an electron acceptor) plays a
35 major role³¹⁻³³. Although significant research efforts have been dedicated to understanding the
36 mechanisms of substrate inhibition³⁴⁻³⁶ and the effects from pore-scale heterogeneities³⁷⁻³⁹ in
37 singularity, the combined effects and the complex interplay between these two disadvantageous
38 rate-limiting mechanisms are not yet understood in detail. Furthermore, while analytical equa-
39 tions allow predicting the dampening effect of mass-transfer limitations on substrate inhibition⁷,
40 the potential occurrence of the effects in-situ and in the presence of pore-scale heterogeneities
41 has not yet been explored.

42 This study considers an extended approach for the modeling of the in-situ biodegradation
43 activities of microbial species that are adversely influenced by substrate inhibition at high con-
44 centration levels. The concept is implemented into a reactive pore network model which allows
45 simulating the heterogeneous transport and reactivity of substrate. The model considers the
46 impact of pore-scale heterogeneities on the distribution and consumption of a toxic substrate
47 in the porous medium and determines the biodegradation capacity of the indigenous microbial
48 population as a function of medium heterogeneity.

49 The purpose of this work is thus to understand the impact of pore-scale heterogeneities on
50 biodegradation of a self-inhibiting substrate. To this end, the numerical reactive pore network
51 model (PNBRNS) introduced in Gharasoo et al.⁹ was upgraded and then used to theoret-

52 ically test the hypothesis of whether pore-scale heterogeneities improve biodegradation of a
53 self-inhibiting substrate. The new, upgraded program (now called Two-dimensional Reactive
54 Pore Network or RePoNet2D) is equally capable of building two-dimensional homogeneous or
55 heterogeneous pore networks, accepting a wide range of pore-scale heterogeneities generated by
56 a pore size distribution and a spatial correlation length, offering a reactive transport platform
57 where an arbitrary combination of reactions can be simulated.

58 This article is structured as follows: first we define the model equations and the underlying
59 assumptions. Then, we describe the construction of heterogeneous pore networks and the
60 simulated scenarios. Simulation results and model solution are presented and discussed at the
61 end.

62 2 Material and Methods

63 The pore network assembly as well as the simulation of flow and transport follow the previous
64 work of Gharasoo et al.⁹ where the details are thoroughly explained. Here, we present only a
65 brief overview of the techniques with some further details in the Supporting Information.

66 2.1 Pore network assembly

67 The model describes the porous medium structure as a two-dimensional network of intercon-
68 nected pores in which every single pore has its own individual characteristics. Each pore is
69 represented as a cylindrical micro tube (Supporting Information Fig. S1). All pores of the
70 network have identical lengths, but the radius of each pore is assigned individually thus permit-
71 ting the generation of heterogeneous pore networks. The connecting nodes are considered to be
72 volumeless while each pore is treated as a finite volume. The network has a regular hexagonal
73 or honeycomb structure since every three pores are connected at a 120° angle in respect to each
74 other (Supporting Information Fig. S1). This forms a two-dimensional pore network with coordi-
75 nation number 3 which is in the range of 2 to 5 suggested as (effective) coordination numbers
76 in the topological analyses of natural porous media⁴⁰. More details on the structure of the pore
77 network are provided in Gharasoo et al.⁹, section 2.2.

78 2.2 Flow and transport model

79 The dynamics of a contaminant inside a porous medium usually include contaminant transport
80 (advection and diffusion) and reactivity (or biodegradation), and are described by the well-
81 established advection-diffusion-reaction equation⁴¹:

$$\frac{\partial c}{\partial t} = -\vec{u} \cdot \vec{\nabla} c + D \nabla^2 c - R(c) \quad (1)$$

82 where $t[T]$ denotes time, $c[ML^{-3}]$ the contaminant bulk concentration in the system, $D[L^2T^{-1}]$
 83 the diffusion coefficient of contaminant, and $\vec{u}[LT^{-1}]$ the laminar fluid velocity vector described
 84 by Hagen-Poiseuille equation $u = \frac{\pi r^2 \Delta p}{8 \nu l}$ where r is the pore radius, Δp the pressure difference
 85 along the pore ends, ν the fluid viscosity, and l the length of pore. Fixed boundary conditions
 86 (or fixed pressure heads) were considered at the inlet and the outlet, or the left and the right
 87 medium boundaries respectively. Zero-flux boundary conditions were applied to the lower and
 88 upper boundaries (or at medium walls). The fluid flow and thus the solute transport are from left
 89 to right. For further details on the numerical computations of the flow and the transport see Gha-
 90 rasoo et al.⁹, section 2.3. The consumption rate of a substrate/contaminant $R(c)[ML^{-3}T^{-1}]$,
 91 described here by a general degradation rate term, is a function of the substrate bioavailable
 92 concentration and the degradation capacity of the bacteria inhabiting the medium taking the
 93 form of one of the kinetic models described below.

94 2.3 Substrate degradation models

95 2.3.1 Michaelis-Menten

96 Michaelis-Menten kinetics⁴² is the simplest form of enzymatic reaction rate law describing the
 97 breakdown of an organic compound due to microbial activity:

$$R(c) = q_{max} \frac{c}{c + K_m} \quad (2)$$

98 with $c[ML^{-3}]$ as substrate bulk concentration, $K_m[ML^{-3}]$ as substrate half-saturation constant,
 99 and $q_{max}[ML^{-3}T^{-1}]$ as maximum volumetric degradation rate. Note that c here is equal to
 100 bioavailable concentration $c_b[ML^{-3}]$ since no other rate-limiting step is present. We consider
 101 all other potentially rate-limiting compounds (e.g., a suitable electron acceptor) to be abundant
 102 at sufficiently high concentrations to avoid additional rate limitations.

103 2.3.2 Bioavailability limitations

104 Best⁴³ described the substrate degradation when a linear mass-transfer term links the bioavail-
 105 able portion of the substrate to its bulk concentration^{44,45}. Contaminants and bacteria are
 106 usually distributed differently in the polluted soil, and the microbial uptake of a contaminant
 107 depends on its bioavailability. The bioavailable concentration $c_b[ML^{-3}]$ is a fraction of the
 108 concentration of contaminant at bulk concentration c . The exchange rate between the bulk and

109 bioavailable phases is usually expressed by a linear driving force model and commonly referred
 110 to as ‘the penetration rate of substrate into the cells’ or bioavailability equation ^{7,45}:

$$r_{ex} = k_{tr}(c - c_b) \quad (3)$$

111 where k_{tr} [T^{-1}] is the limiting mass-transfer coefficient controlling contaminant bioavailability.
 112 At (quasi-) steady state conditions, the rate of contaminant exchange r_{ex} is considered equal to
 113 its degradation rate. The linear driving force model Eq. (3) can therefore be combined with the
 114 Michaelis-Menten kinetics (Eq. (2)) leading to the following equation ⁴³,

$$R(c) = \frac{k_{tr}}{2}(c + K_m + q_{max}/k_{tr}) \left(1 - \sqrt{1 - \frac{4cq_{max}/k_{tr}}{(c + K_m + q_{max}/k_{tr})^2}} \right) \quad (4)$$

115 where the contaminant degradation rate in the presence of small-scale bioavailability restrictions
 116 is expressed as a function of its bulk concentration. k_{tr} can either be considered as constant ^{11,46}
 117 or determined from an upscaled model. The pore network case studies here use the following
 118 equation suggested by Hesse et al. ⁴⁷ to describe the intra-pore bioavailability limitation effects
 119 inside a cylindrical pore

$$k_{tr} = \frac{\pi^2}{4} \frac{D_p a_v}{r} \quad (5)$$

120 where r is the average radius of pore, D_p is the intra-pore diffusion coefficient, and a_v [L^{-1}] is
 121 the specific surface area of the porous matrix. It was assumed that bacteria access only the
 122 bioavailable fraction of substrate at the close vicinity of the biofilm, relying on the substrate
 123 mass transfer to their location at the pore wall (see the Supporting Information Fig. S1). In this
 124 model, intra-pore diffusivity was considered as the main mechanism for limiting mass transfer
 125 between the bulk concentration at the plume and the bioavailable concentration at the pore
 126 walls where the microbial biomass is located ⁹.

127 2.3.3 Non-competitive inhibition

128 Substrate self-inhibition is described based on the fact that contaminants act as nutrients at
 129 low concentrations while they exhibit toxicity at high concentrations. There are currently many
 130 modeling approaches to describe the inhibitory effect of substrate on microbial/enzyme activity.
 131 The variation of the suggested equations for different inhibition kinetics (competitive, non-
 132 competitive, self-toxicity, mixed-toxicity, etc) have been already reviewed extensively in Ramsay

133 and Tipton⁴⁸ and Yoshino and Murakami². Many of these equations modified and adjusted the
 134 classical inhibition model suggested by Haldane¹:

$$R(c) = q_{max} \frac{c k_i}{(c + K_m)(c + k_i)} \quad (6)$$

135 with $k_i [ML^{-3}]$ as inhibition constant. Eq. (6) was proposed to describe the non-competitive in-
 136 hibition of a substrate on the enzyme metabolism^{49,50} and has been regularly used for modeling of
 137 inhibitory effects in reactive transport models⁵¹. The presence of a maxima at $Smax_H [ML^{-3}] =$
 138 $\sqrt{k_i K_m}$ in the Haldane equation means that the rates are lower at both concentration levels
 139 lower and higher than $Smax_H$ ⁷. In fact, at very high contaminant concentrations the rates
 140 are inversely proportional to the concentrations $R(c) = \frac{k_i}{c}$. The maximum observed degra-
 141 dation rate is calculated from the second derivative of the Eq. (6) as $R_{max} [ML^{-3}T^{-1}] =$
 142 $1/(1 + \sqrt{K_m/k_i})^2$.

143 2.3.4 Inhibition and bioavailability

144 To account for the combined effect of both mass-transfer limitation and self-inhibition together,
 145 the following system of ordinary differential equations (ODEs) must be solved either numerically
 146 or analytically:

$$\begin{cases} r_{ex} = k_{tr}(c - c_b) & (7a) \\ R(c) = q_{max} \frac{c_b k_i}{(c_b + K_m)(c_b + k_i)} & (7b) \end{cases}$$

147

148 Gharasoo et al.⁷ solved the above system of equations and presented an analytical closed
 149 formulation for calculating substrate degradation rates under the effects of both mechanisms. It
 150 was shown that in presence of mass-transfer limitations, the maximum degradation rate R_{max}
 151 of a self-inhibiting substrate was attained at higher concentration levels. This is due to the
 152 dampening effects that mass-transfer limitations impose on a substrate's toxicity (i.e. toxicity
 153 is reduced at enzyme level because lower concentrations of substrate are available due to mass-
 154 transfer effects).

155 2.4 Pore network case studies

156 The case studies were designed to facilitate the assessment of the role of pore-scale heterogeneities
 157 on the total biodegradation capacity of a porous medium. In this study, two aspects were

158 used to generate the desired spatial heterogeneity: a normal distribution of pore-sizes (or a
159 pore-size histogram) and a spatial correlation length^{9,28}. Pore networks were constructed using
160 normal distributions of the pore sizes described with an average pore radius and various standard
161 deviations. Similar to Nowak et al.⁵², correlation length was used in an exponential covariance
162 function for building the spatially correlated heterogeneous pore networks using the FFT-based
163 random field generating technique by Dietrich and Newsam⁵³. For further information see
164 Gharasoo et al.⁹, section 3.4. Note that there is no limitations in generating different 2D
165 heterogeneous scenarios at any desired size using the techniques explained above.

166 In analogy to Gharasoo et al.⁹, six heterogeneously different scenarios were generated as
167 the result of combining two standard deviations (45 and 70 μm) and three correlation lengths
168 (1, 2.5, and 5 mm). As an example, a generated random realization from every pore-network
169 scenario together with their associated histograms (of the pore-size distribution) are shown in
170 Fig. 1. The generated pore network scenarios are an extension of the previous work of Gharasoo
171 et al.⁹ and the techniques employed here have been previously shown capable of addressing
172 structural heterogeneities observed in soil environments^{27,54}. A homogeneous pore network was
173 also designed to serve as a basis for comparison. The homogeneous pore network was constructed
174 with identical pores of the length of 1 mm and radius of 160 μm . The heterogeneous pore networks
175 were created using the same pore length but different pore radii distributions and correlation
176 lengths as described above. For each heterogeneous scenario, five realizations with the same
177 geostatistical properties were generated. The final results for each heterogeneous scenario are
178 calculated as the averages between all the realizations from that scenario. In all scenarios a
179 continuous and steady supply of a single substrate with the concentration of 1.55 μM , the half-
180 saturation constant $K_m = 0.261\mu\text{M}$, and the inhibition constant $k_i = 1.5K_m$ (for inhibitory
181 mechanisms), was supplied to the system from the inlet boundary at the left side. The substrate
182 degraded as a result of exposure to the biomass in the pores, and discharged from the outlet
183 at the right boundary. The outlet concentrations at steady-state (C_{out}) and the normalized
184 difference between the outlet and inlet concentrations ($\Delta C/C_{in}$) were considered as a measure
185 for biodegradation capacity for the scenarios. Note that the inlet concentration was kept constant
186 throughout the simulation.

187 The pore network models ran until a constant concentration at the outlet was measured and
188 the system reached steady-state. The governed equations were solved for a homogeneous pore
189 network (similar to a homogenized artificial soil), and six heterogeneous pore network scenar-
190 ios (similar to undisturbed soil). The degradation of contaminant under the above mentioned

191 reaction kinetics (Michaelis-Menten Eq. (2), Best Eq. (4), Haldane Eq. (6), and the cumulative
192 effects of bioavailability and inhibition Eq. (7)) for every scenario (and the realizations) was sim-
193 ulated (total of 124 compound profiles for all the heterogeneous scenarios plus the homogeneous
194 scenario).

195 Inside the pore networks, the inoculated biomass was assumed immobile and attached to
196 the solid matrix forming a uniform biofilm on the pore walls (similar to the assumptions in
197 Gharasoo et al.⁹, Lopez-Peña et al.⁵⁵). Note that unlike Lopez-Peña et al.⁵⁵ the biomass in
198 our system was assumed fixed for the sake of simplicity and the reasons explained in the next
199 paragraph. According to the experimental observations of Harms and Zehnder⁵⁶ from which
200 the current model parameter values are taken (listed in the Supporting Information, Table S1),
201 bacterial motilities (chemotaxis) or their detachment off the solid matrix did not occur in the
202 experiments. Detachment was thus considered insignificant due to negligible shear stresses in
203 the medium as the result of slow flow velocities (about 1.2 mm/s).

204 Since the residence time of solutes in the pore network was much shorter than the typical
205 time scale for growth, the biofilm growth or decay was assumed insignificant (similar to Jung
206 and Meile⁵⁷). Given that the experimental measurements were performed after the system
207 reached steady-state⁵⁶, the model looks at a snapshot of experiment where the given biomass
208 densities (and other reported parameter values in support information, Table S1) were measured.
209 Allowing the system to balance itself (through the growth and decay) leads to dissimilar amount
210 of final biomass at each scenario (or even realization) and compromises the validity of the
211 comparison between the final results. Since the biomass density and the water residence time are
212 initially set equal in all the scenarios (and realizations), to ensure that the observed differences
213 in results are solely due to the heterogeneities and not to the changes of other parameters, it
214 was crucial that biomass densities and water residence times stay fixed in time. Biomass growth
215 or decay may jeopardize this equality and put the presented results under the question whether
216 the observed differences were only due to the differences in pore-size heterogeneities. Moreover,
217 due to the substrate inhibitory effects, it may not necessarily be the primary compound required
218 for the growth.

219 Due to no-growth conditions of biomass in the experiment, biomass surface density ρ_{bac} [ML^{-2}]
220 remained constant during the simulations. For the cylindrical shape of pores q_{max} was calculated
221 as $q_{max} = \rho_{bac} a_v V_{max}$ where a_v [L^{-1}] denotes the specific surface area of the porous matrix equal
222 to $25 \times 10^3 \text{ m}^{-1}$, ρ_{bac} the biomass surface density equal to $4.1 \text{ mg}(\text{protein}) \text{ m}^{-2}$, and V_{max} [T^{-1}]
223 the maximum specific degradation rate equal to $3.27 \times 10^{-2} [\text{mol}(\text{substrate}) \text{ mg}(\text{protein})^{-1} \text{ s}^{-1}]$,

224 measured from the experiments^{9,56}. No further chemical species (e.g., terminal electron accep-
225 tors or additional nutrients) were considered to influence the microbial degradation rates. Only
226 the entering substrate limited the metabolic activity of the microorganisms in case of inhibition.
227 All the pore network scenarios were equal in size and had equal length and width of 8.9 by 3.1
228 cm.

229 2.5 The new tool RePoNet2D

230 The two-dimensional Reactive Pore Network model (RePoNet2D) uses the pore network trans-
231 port code in Gharasoo et al.⁹ and couples it with an internal reactive module similar to that in
232 Gharasoo et al.⁵⁸. Thus, unlike PNBRS⁹ that uses BRNS (The Biogeochemical Reaction Net-
233 work Simulator)⁵⁹ as the internal reactive module, RePoNet2D uses a newly developed reactive
234 module of its own that is more flexible and highly adjustable.

235 For every scenario, we simulated the reactive transport of four substrates each following
236 one of the degradation mechanisms as described above (Eq. (2), Eq. (4), Eq. (6), and Eq. (7)),
237 leading to a system of ordinary differential equations(ODEs) that the internal reactive module
238 of RePoNet2D numerically solves using the ODE suite of MATLAB (ode15s). To speed up the
239 calculations, the Jacobian matrix of the ODE system is analytically calculated and passed to
240 the ode15s. The reactive module is linked to the transport code using an operator splitting
241 technique, similar to the coupling of BRNS to the MATLAB transport code in Gharasoo et al.⁹.
242 In operator (or time) splitting technique which is also known as the sequential non-iterative
243 approach (SNIA), we first solve the transport and then the reaction terms in a sequence for a
244 single time step (similar to e.g., Sun and Duddu⁶⁰). To minimize the splitting error, relatively
245 small time steps were taken following Courant-Friedrichs-Lewy criterion. Since the transport
246 code solves the advection step with an explicit backward Euler technique, taking a small time
247 step was already required.

248 RePoNet2D is highly flexible in allowing users to define any arbitrary set of reaction mecha-
249 nisms. The RePoNet2D reactive module uses parallel-computation to reduce the overall compu-
250 tation time. Compared to codes such as those using modules of different origin (e.g., PNBRS)
251 RePoNet2D provides the advantage that all components are scripted in one environment (MAT-
252 LAB).

253 The computational wall-time for each heterogeneous realization assuming four reactive com-
254 pounds, each following one of the four mechanisms of degradation, was in average about 6 hours
255 on a quad-cores Intel Core i5-4590 CPU at 3.30 GHz with 16GB RAM. Simulating all the 30

256 realizations (five for each of the six heterogeneous scenarios) took approximately 180 hours.
257 The results of the current setup showed relatively small deviations at the end (see Table 1).
258 Therefore, although running the model for a larger number of realizations can be statistically
259 beneficial, we assumed the current number of realizations to be a reasonable compromise between
260 the computational demand and the statistical accuracy.

261 3 Results and Discussion

262 The spatial distributions of rates and concentration profiles during the transient expansion of the
263 substrate plume and at the steady-state are shown in Figs. 2 and 3 for a heterogeneous sample
264 scenario. Results highlight the differences in hot spots of degradation and the spatio-temporal
265 effects of substrate self-inhibition. While in the absence of inhibition effects, highest degradation
266 rates are found at the plume core where substrate concentrations are the highest, degradation
267 of a self-inhibitory substrate is mostly limited to the plume fringes where the concentrations are
268 relatively lower. This leads to the abundance of low rate regions and a larger plume size for the
269 substrate with self-inhibitory effects. The average outlet concentration at steady state was used
270 as a reference for the total substrate consumption, with lower outlet concentrations indicating
271 a higher total in-situ degradation rate, and vice versa.

272 Table 1 summarizes the outlet concentrations from all the case studies. While the pore-
273 size heterogeneities had an adverse effect on degradation of a typical (non-inhibiting) substrate
274 (reflected by increased outlet concentrations), the same heterogeneities slightly improved the
275 degradation of a self-inhibiting substrate. The variations in both pore-size and correlation length
276 impacted the variability of measured outlet concentrations, where the effect from correlation
277 length was found to be stronger in comparison, indicated by proportionally larger confidence
278 intervals as shown in Fig. 5.

279 3.1 Bioavailability limitations in the absence of inhibition

280 In the absence of substrate inhibition, pore-scale mass-transfer limitations can have only a
281 negative effect on the total degradation regardless of whether structural heterogeneities are
282 present or not. This is also evident from the theoretical analysis of the rate expressions showing
283 that the degradation rate of a contaminant following Best kinetics is consistently lower than the
284 one following Michaelis-Menten kinetics due to the extra linear mass-transfer term Eq. (3)^{7,44}.

285 For a pore of an average size (radius of 160 μm), the mass-transfer limiting coefficient was
286 calculated as $k_{tr} = 0.231\text{s}^{-1}$ according to Eq. (5). Solution of Eq. (4) reveals that at such a rela-

287 tively high k_{tr} -value the bioavailability restrictions are mildly noticeable, therefore the observed
288 differences between Michaelis-Menten and Best kinetics were insignificant in a homogeneous
289 pore network⁹. A comparison between the steady-state solution of Michaelis-Menten and Best
290 kinetics in a heterogeneous pore network scenario also indicates that the differences between
291 final concentration profiles were relatively small (data not shown). As shown in Table 1, the
292 steady outlet concentrations for Best kinetics were slightly higher meaning, as expected, the
293 mass-transfer limitations reduced the total in-situ biodegradation.

294 3.2 Spatial and temporal effects of substrate inhibition

295 In the presence of inhibition, not only were the rates at any substrate concentration lower
296 than, or at best equal to the non-inhibited rates, but also the maximum degradation rate R_{max}
297 was considerably lower than the maximum volumetric degradation rate q_{max} (see the differences
298 between Eq. (6) and Eq. (2)). The toxicity effects exposed by a self-inhibiting substrate causes its
299 overall degradation rate to be consistently lower than a non-inhibiting counterpart that follows
300 Michaelis-Menten kinetics. This explains the results in Fig. 2 where for a typical non-inhibiting
301 substrate the consumption rates within the pore network scenario were consistently higher and
302 thus lower outlet concentrations were measured (Table 1).

303 The high concentrations of substrate are logically observed around the inlet boundary. As
304 such, the zones with highest degradation rates were found close to the inlet for a typical (non-
305 inhibiting) substrate (Fig. 2: left column). The further expansion of contaminant plume into
306 the medium only extended this pattern and did not change its initial form at earlier times.
307 However, for a self-inhibiting substrate the highest rates were detected at the areas near the tip
308 of the plume or at the fringes located far away from the inlet (Fig. 2: right column). In these
309 zones, the concentration of substrate is reduced to some optimal levels due to the dispersion
310 and the consumption at initial stages. By the expansion of the plume, the zones with high
311 degradation rates were observed to shift away from the main flow stream towards the remote
312 areas such as isolated segments of small pores where due to lower hydraulic conductivities a lower
313 concentration of substrate is supplied. At steady state, high degradation rates were detected
314 at the plume fringes, in the areas relatively close to the outlet, and in isolated patches of small
315 pores.

3.3 Bioavailability limitations in the presence of inhibition

Opposite to the observations in Section 3.1 which were predictable and theoretically straightforward, no intuitive understanding exists between the two more complicated degradation kinetics: non-competitive inhibition Eq. (6) and inhibition plus bioavailability Eq. (7). Within the pore networks, the distribution of a substrate due to advection and diffusion develops variously distributed gradients of concentration along the longitudinal and transverse directions. Substrate degradation along those pathways, especially in the presence of structural heterogeneities, makes it even more complicated to a priori predict the cumulative effects of pore-scale mass-transfer limitations, pore-scale heterogeneity and self-inhibition. Small-scale bioavailability restrictions can be either rate-limiting or beneficial to the degradation of a substrate as a result of the interplay between several factors such as contaminant inlet concentration, the initial level of contaminant toxicity to the biomass in pores, and the spatial distribution of the pores in the pore network⁷.

Pore network simulation results show that inhibition in the presence of bioavailability limitations led to marginally higher degradation rates in both, homogeneous and heterogeneous pore networks, compared to the scenarios where only inhibition was present (Table 1). Noting that the Best kinetics in the absence of inhibitory effects consistently led to lower rates than Michaelis-Menten kinetics, the results presented in this study show that it is possible that bioavailability restrictions are able to facilitate the consumption of a self-inhibiting substrate. In this study, very small differences were noticed between the results of non-competitive inhibition and inhibition plus bioavailability kinetics. This might be due to the relatively high values of the mass-transfer coefficient k_{tr} used in this study, which ultimately led to low dampening effects on the substrate toxicity. As shown by Eq. (5), the k_{tr} value is inversely proportional to the mean pore-size value which is relatively large (160 μm) for generated pore networks in this study. It is speculated that in cases where the mass-transfer limitations are stronger (i.e. k_{tr} is smaller), the resulting differences between degradation rates will be more pronounced.

In a separate method of evaluation, the histogram of the degradation rates inside a heterogeneous pore network for both kinetics: non-competitive inhibition Eq. (6) and inhibition plus bioavailability Eq. (7) is illustrated (Supporting Information, Fig. S2). It is clear that the number of pores with higher in-situ degradation rates is slightly higher for the case of inhibition plus bioavailability. This additionally explains the slight differences observed between the average outlet concentrations (Table 1).

348 3.4 Pore-scale homogeneity vs. heterogeneity

349 As the concentration of an inhibiting substrate inside a medium decreases away from the inlet,
350 we observe higher degradation rates towards the outlet. In the homogeneous case, the trend is
351 continuous and steady while in the heterogeneous cases, the presence of preferential flow paths
352 and hotspots of degradation produce a heterogeneous pattern that is largely influenced by the
353 spatial alignment of the pore-network heterogeneity (Supporting Information, Fig. S3). It also
354 takes longer for a heterogeneous case to reach steady-state compared to the homogeneous case
355 Fig. 4. In a heterogeneous medium, this is mainly due to irregular distribution of pores of
356 different sizes that creates hotspots and preferential flow paths. In the presence of inhibition,
357 the lag is even greater since the favorable zones for degradation change as the plume extends
358 (see Fig. 2). Both rate profiles and concentration profiles support the findings that the presence
359 of inhibition in general reduce the rates significantly, irrespective of the presence of small-scale
360 bioavailability limitations or pore-scale heterogeneities.

361 The heterogeneous pore networks here demonstrate the effects from structural heterogeneity
362 as another limiting mechanism similar to the small-scale mass-transfer limitations⁴⁷. In case of
363 zero inhibition, lower degradation rates were observed in the presence of mass-transfer limitations
364 or structural heterogeneities⁷. In the presence of inhibition effects, structural heterogeneities are
365 predicted to lead to a reduced access of microorganisms to the toxic level of contaminant similarly
366 to the effect caused by mass-transfer (or bioavailability) limitations. The only difference is that
367 in homogeneous systems the mass-transfer limitations happen mainly at the intra-pore level (or
368 across the cell membrane) while the effects from structural heterogeneities occur in addition to
369 those at the inter-pore level⁹ (see Supporting Information Fig. S1). In the case of inhibition,
370 although the relationships become more complex and less correlated, it was possible with the
371 help of pore network modeling to show the stimulating effect of pore-scale heterogeneities on
372 the degradation of a self-inhibiting substrate (see Table 1 and Fig. 5). Fig. 5 further shows
373 that double rate-limiting effects caused by both small-scale mass-transfer limitations and pore-
374 size heterogeneity can further improve the rates. The observed effects from heterogeneities,
375 though small, are consistently positive (about 2% as seen in Fig. 5). To keep it in line with the
376 experimental reference⁵⁶ and the previous modeling study⁹, we used the same set of parameters
377 values. Due to the specific combination of the parameter values in this study, for example a
378 relatively high values of mass-transfer coefficient k_{tr} (calculated by Eq. (5)), we did not notice
379 a significant dampening effect on the substrate toxicity. In addition, we did not observe a wide

380 range of toxic concentrations in these scenarios and the changes in substrate concentration were
381 within the same order of magnitude. The effect from pore-scale heterogeneities might turn
382 more pronounced if a different combination of kinetic parameters (k_{tr} , k_i , q_{max} , and K_m) are
383 used, particularly at sufficiently small k_{tr} values. It is however beyond the aim of this study
384 to determine and explore further potential combinations of parameter values. It is also noted
385 that the standard variation of results (C_{out} or $\Delta C/C_{in}$) is higher both, in the presence of pore-
386 scale mass-transfer limitations and at more heterogeneous pore network scenarios (generated by
387 higher pore-size variance and larger correlation length).

388 It has been traditionally believed that structural heterogeneities hinder the bacterial access
389 to substrate and therefore reduce the overall degradation capacity of a medium. While this is
390 true for a typical non-inhibiting substrate, the results for a self-inhibiting substrate was shown
391 to evince the possibility of gaining a total higher degradation rate in the presence of structural
392 heterogeneities (Table 1). In order to be able to find the relative impact of each parameter on
393 the overall degradation efficiency, it is required to perform a global sensitivity analysis (GSA)
394 on the model in a sufficiently large space of parameter values covered by a uniform sampling
395 technique such as Latin-hyper cube or Sobol sequence^{46,61,62}. To this end, the model requires
396 to run at least for 1000 different combinations of the parameter values for every heterogeneous
397 scenario. The present study only aims to show the general possibility of the concept, thus a full
398 analysis of the parameters is beyond the scope of this study.

399 3.5 Practical environmental implications

400 The current study bridges the gap between geo-related limitations (small-scale mass-transfer
401 limitations and pore-scale heterogeneities) and biological limitations (substrate self-inhibition)
402 and explores their interactions when both limitations are present. The numerical simulations
403 here thus aimed to unravel the extent of influence that typical pore-size heterogeneities have on
404 natural attenuation of self-inhibiting contaminants, and to compare the results with previous
405 studies where substrate inhibition was neglected. Structural heterogeneities, similar to small-
406 scale bioavailability limitations, were always assumed to reduce the in-situ rate of substrate
407 biodegradation. In this context, the arguments were concentrated on the role of structural
408 heterogeneities as a limiting and negatively influencing factor that further reduce the microor-
409 ganisms access to a substrate. The presence of substrate inhibition has a counter-intuitive effect
410 since higher concentrations of substrate impose a negative impact on the enzymes metabolic
411 activity. The results from this study revealed that in the presence of substrate inhibition, higher

412 biodegradation rates can be achieved in a more heterogeneous medium. Moreover, the pres-
413 ence of small-scale mass-transfer limitations additionally improved the degradation rates of a
414 self-inhibiting substrate in such scenarios.

415 The current findings not only link the descriptions of pore-scale heterogeneities to substrate
416 inhibition, but also have biotechnological and bioengineering applications in real life, leading
417 to a new view on the design of biofilters and bioremediation sites. First, the medium hetero-
418 geneities can be utilized in order to attain higher degradation rates at toxic levels of contam-
419 inant concentrations. At high concentrations, the optimized use of mass-transfer limitations
420 can therefore reduce the initial toxicity of contaminants to microorganisms, increase the bio-
421 consumption rates and provide a lower, sustainable level of contaminant concentrations for the
422 next stages of bioremediation. When the contaminant concentrations decrease to a lower level,
423 the subsequent shifting to a less heterogeneous medium would further elevate the contaminant
424 bioremediation. In this respect, designing a biofilter for a self-inhibiting contaminant requires
425 a sequential decrease of heterogeneity from inlet towards outlet given the high concentrations
426 at inlet are initially hazardous to bacteria. Secondly, while the usual solution of dealing with
427 toxic concentrations of contaminant includes the dilution of the mixture, which in turn results
428 in a pollution of even more water resources, the practical use of the presented findings can lead
429 to the design of technologically sophisticated systems in which an advanced use of pore-scale
430 heterogeneities ensures higher biodegradation efficiency. Thirdly, since highest degradation rates
431 were observed at the tip of a self-inhibiting substrate plume Fig. 2, a pulse injection strategy of
432 the toxic substrate into the media would result in a better degradation efficiency in comparison
433 to a continuous injection.

434 Compound-specific isotope analysis (CSIA) has been intensively used for assessing contami-
435 nant fate and transport in ecosystems. Small-scale bioavailability limitations have been shown
436 to be responsible for the differences observed between the measured and the expected (or actual)
437 isotopic signatures^{63–65}. Extension of this modeling approach by including substrate isotopic
438 fractionation to the model might provide a theoretical clue about the impact that soil het-
439 erogeneities or substrate inhibition have on the observed isotopic signatures in the natural or
440 man-made environments.

441 Acknowledgments

442 This research was funded by the European Union Marie Curie Host Early Stage Training (EST)
443 through grant MC-EST 20984 (RAISEBIO). Additional funding was provided by the Canada

444 Excellence Research Chair (CERC) program in Ecohydrology group at UWaterloo.

445 Supporting Information

446 Supporting Information is available containing an additional overview on used parameters and
447 additional simulation results.

448 References

- 449 [1] Haldane, J. B. S. *Enzymes*; Longmans, Green, and co: New York, 1930; pp 28–53.
- 450 [2] Yoshino, M.; Murakami, K. Analysis of the substrate inhibition of complete and partial types. *Springerplus* **2015**, *4*,
451 292.
- 452 [3] Astals, S.; Peces, M.; Batstone, D.; Jensen, P.; Tait, S. Characterising and modelling free ammonia and ammonium
453 inhibition in anaerobic systems. *Water Res* **2018**, *143*, 127–135.
- 454 [4] Vela, J. D.; Dick, G. J.; Love, N. G. Sulfide inhibition of nitrite oxidation in activated sludge depends on microbial
455 community composition. *Water Res* **2018**, *138*, 241–249.
- 456 [5] Hanzel, J.; Thullner, M.; Harms, H.; Wick, L. Y. Walking the tightrope of bioavailability: growth dynamics of PAH
457 degraders on vapour-phase PAH. *Microb Biotechnol* **2012**, *5*, 79–86.
- 458 [6] Lauchnor, E. G.; Semprini, L. Inhibition of phenol on the rates of ammonia oxidation by *Nitrosomonas europaea* grown
459 under batch, continuous fed, and biofilm conditions. *Water Res* **2013**, *47*, 4692–4700.
- 460 [7] Gharasoo, M.; Centler, F.; Van Cappellen, P.; Wick, L. Y.; Thullner, M. Kinetics of Substrate Biodegradation under
461 the Cumulative Effects of Bioavailability and Self-Inhibition. *Environ Sci Technol* **2015**, *49*, 5529–5537.
- 462 [8] Park, W.; Jeon, C.; Cadillo, H.; DeRito, C.; Madsen, E. Survival of naphthalene-degrading *Pseudomonas putida* NCIB
463 9816-4 in naphthalene-amended soils: toxicity of naphthalene and its metabolites. *Appl Microbiol Biotechnol* **2004**,
464 *64*, 429–435.
- 465 [9] Gharasoo, M.; Centler, F.; Regnier, P.; Harms, H.; Thullner, M. A reactive transport modeling approach to simulate
466 biogeochemical processes in pore structures with pore-scale heterogeneities. *Environ Model Softw* **2012**, *30*, 102–114.
- 467 [10] Prommer, H.; Anneser, B.; Rolle, M.; Einsiedl, F.; Griebler, C. Biogeochemical and Isotopic Gradients in a BTEX/PAH
468 Contaminant Plume: Model-Based Interpretation of a High-Resolution Field Data Set. *Environ Sci Technol* **2009**, *43*,
469 8206–8212.
- 470 [11] Sun, F.; Mellage, A.; Gharasoo, M.; Melsbach, A.; Cao, X.; Zimmermann, R.; Griebler, C.; Thullner, M.; Cirpka, O. A.;
471 Elsner, M. Mass-Transfer-Limited Biodegradation at Low Concentrations—Evidence from Reactive Transport Model-
472 ing of Isotope Profiles in a Bench-Scale Aquifer. *Environ Sci Technol* **2021**, *55*, 7386–97.
- 473 [12] Attinger, S.; Dimitrova, J.; Kinzelbach, W. Homogenization of the transport behavior of nonlinearly adsorbing pollu-
474 tants in physically and chemically heterogeneous aquifers. *Adv Water Resour* **2009**, *32*, 767–777.
- 475 [13] Borch, T.; Kretzschmar, R.; Kappler, A.; Cappellen, P. V.; Ginder-Vogel, M.; Voegelin, A.; Campbell, K. Biogeochem-
476 ical Redox Processes and their Impact on Contaminant Dynamics. *Environ Sci Technol* **2010**, *44*, 15–23.
- 477 [14] Rolle, M.; Le Borgne, T. Mixing and Reactive Fronts in the Subsurface. *Rev Mineral Geochem* **2019**, *85*, 111–142.
- 478 [15] Wright, E. E.; Richter, D. H.; Bolster, D. Effects of incomplete mixing on reactive transport in flows through hetero-
479 geneous porous media. *Phys Rev Fluids* **2017**, *2*, 114501.
- 480 [16] Jiménez-Martínez, J.; de Anna, P.; Tabuteau, H.; Turuban, R.; Borgne, T. L.; Méheust, Y. Pore-scale mechanisms for
481 the enhancement of mixing in unsaturated porous media and implications for chemical reactions. *Geophys Res Lett*
482 **2015**, *42*, 5316–5324.
- 483 [17] McMillan, L. A.; Rivett, M. O.; Wealthall, G. P.; Zeeb, P.; Dumble, P. Monitoring well utility in a heterogeneous
484 DNAPL source zone area: Insights from proximal multilevel sampler wells and sampling capture-zone modelling. *J*
485 *Contam Hydrol* **2018**, *210*, 15 – 30.
- 486 [18] Puigserver, D.; Carmona, J. M.; Cortés, A.; Viladevall, M.; Nieto, J. M.; Grifoll, M.; Vila, J.; Parker, B. L. Subsoil
487 heterogeneities controlling porewater contaminant mass and microbial diversity at a site with a complex pollution
488 history. *J Contam Hydrol* **2013**, *144*, 1 – 19.

- 489 [19] Portell, X.; Pot, V.; Garnier, P.; Otten, W.; Baveye, P. C. Microscale Heterogeneity of the Spatial Distribution of
490 Organic Matter Can Promote Bacterial Biodiversity in Soils: Insights From Computer Simulations. *Front Microbiol*
491 **2018**, *9*, 1583.
- 492 [20] Schmidt, S. I.; Kreft, J.-U.; Mackay, R.; Picioreanu, C.; Thullner, M. Elucidating the impact of micro-scale heteroge-
493 neous bacterial distribution on biodegradation. *Adv Water Resour* **2018**, *116*, 67–76.
- 494 [21] Thullner, M.; Regnier, P. Microbial Controls on the Biogeochemical Dynamics in the Subsurface. *Rev Mineral Geochem*
495 **2019**, *85*, 265–302.
- 496 [22] König, S.; Worrlich, A.; Centler, F.; Wick, L. Y.; Miltner, A.; Kästner, M.; Thullner, M.; Frank, K.; Banitz, T.
497 Modelling functional resilience of microbial ecosystems: Analysis of governing processes. *Environ Model Softw* **2017**,
498 *89*, 31–39.
- 499 [23] Deschesne, A.; Pallud, C.; Grundmann, G. L. In *The Spatial Distribution of Microbes in the Environment*;
500 Franklin, R. B., Mills, A. L., Eds.; Springer Netherlands: Dordrecht, 2007; pp 87–107.
- 501 [24] König, S.; Köhnke, M. C.; Firlé, A.-L.; Banitz, T.; Centler, F.; Frank, K.; Thullner, M. Disturbance Size Can Be
502 Compensated for by Spatial Fragmentation in Soil Microbial Ecosystems. *Front Ecol Evol* **2019**, *7*, 290.
- 503 [25] Nunan, N.; Wu, K.; Young, I. M.; Crawford, J. W.; Ritz, K. Spatial distribution of bacterial communities and their
504 relationships with the micro-architecture of soil. *FEMS Microbiol Ecol* **2003**, *44*, 203–215.
- 505 [26] Sookhak Lari, K.; Davis, G. B.; Rayner, J. L.; Bastow, T. P.; Puzon, G. J. Natural source zone depletion of LNAPL:
506 A critical review supporting modelling approaches. *Water Res* **2019**, *157*, 630–646.
- 507 [27] Stolpovsky, K.; Gharasoo, M.; Thullner, M. The Impact of Pore-Size Heterogeneities on the Spatiotemporal Variation
508 of Microbial. *Soil Sci* **2012**, *177(2)*, 98–110.
- 509 [28] Brovelli, A.; Carranza-Diaz, O.; Rossi, L.; Barry, D. Design methodology accounting for the effects of porous medium
510 heterogeneity on hydraulic residence time and biodegradation in horizontal subsurface flow constructed wetlands.
511 *Ecological Engineering* **2011**, *37*, 758–770.
- 512 [29] Maloszewski, P.; Wachniew, P.; Czupryński, P. Study of hydraulic parameters in heterogeneous gravel beds: Con-
513 structed wetland in Nowa Słupia (Poland). *Journal of Hydrology* **2006**, *331*, 630–642.
- 514 [30] Suliman, F.; Futsaether, C.; Oxaal, U. Hydraulic performance of horizontal subsurface flow constructed wetlands for
515 different strategies of filling the filter medium into the filter basin. *Ecological Engineering* **2007**, *29*, 45–55.
- 516 [31] Bauer, R. D.; Maloszewski, P.; Zhang, Y.; Meckenstock, R. U.; Griebler, C. Mixing-controlled biodegradation in a
517 toluene plume — Results from two-dimensional laboratory experiments. *Journal of Contaminant Hydrology* **2008**, *96*,
518 150–168.
- 519 [32] Bauer, R. D.; Rolle, M.; Bauer, S.; Eberhardt, C.; Grathwohl, P.; Kolditz, O.; Meckenstock, R. U.; Griebler, C.
520 Enhanced biodegradation by hydraulic heterogeneities in petroleum hydrocarbon plumes. *Journal of Contaminant*
521 *Hydrology* **2009**, *105*, 56–68.
- 522 [33] Robinson, C.; Brovelli, A.; Barry, D.; Li, L. Tidal influence on BTEX biodegradation in sandy coastal aquifers.
523 *Advances in Water Resources* **2009**, *32*, 16–28.
- 524 [34] Adkar, B. V.; Bhattacharyya, S.; Gilson, A. I.; Zhang, W.; Shakhnovich, E. I. Substrate inhibition imposes fitness
525 penalty at high protein stability. *PNAS* **2019**, *116*, 11265–11274.
- 526 [35] Reed, M. C.; Lieb, A.; Nijhout, H. F. The biological significance of substrate inhibition: A mechanism with diverse
527 functions. *BioEssays* **2010**, *32*, 422–429.
- 528 [36] Robin, T.; Reuveni, S.; Urbakh, M. Single-molecule theory of enzymatic inhibition. *Nat Commun* **2018**, *9*, 779.
- 529 [37] Blunt, M. J.; Bijeljic, B.; Dong, H.; Gharbi, O.; Iglauer, S.; Mostaghimi, P.; Paluszny, A.; Pentland, C. Pore-scale
530 imaging and modelling. *Adv Water Resour* **2013**, *51*, 197–216.
- 531 [38] de Anna, P.; Jiménez-Martínez, J.; Tabuteau, H.; Turuban, R.; Le Borgne, T.; Derrien, M.; Méheust, Y. Mixing
532 and Reaction Kinetics in Porous Media: An Experimental Pore Scale Quantification. *Environ Sci Technol* **2014**, *48*,
533 508–516.
- 534 [39] Pedersen, L. L.; Smets, B. F.; Dechesne, A. Measuring biogeochemical heterogeneity at the micro scale in soils and
535 sediments. *Soil Biol Biochem* **2015**, *90*, 122–138.
- 536 [40] Vogel, H.-J.; Roth, K. Quantitative morphology and network representation of soil pore structure. *Adv Water Resour*
537 **2001**, *24*, 233–242.
- 538 [41] Clairambault, J. In *Encyclopedia of Systems Biology*; Dubitzky, W., Wolkenhauer, O., Cho, K.-H., Yokota, H., Eds.;
539 Springer New York: New York, NY, 2013; pp 1817–1817.

- 540 [42] Michaelis, L.; Menten, M. Die Kinetik der Invertinwirkung. *Biochem Z* **1913**, *49*, 333–369.
- 541 [43] Best, J. The inference of intracellular enzymatic properties from kinetic data obtained on living cells: Some kinetic
542 considerations regarding an enzyme enclosed by a diffusion barrier. *J Cell Comp Physiol* **1955**, *46*, 1–27.
- 543 [44] Bosma, T. N.; Middeldorp, P. J.; Schraa, G.; Zehnder, A. J. Mass Transfer Limitation of Biotransformation: Quanti-
544 fying Bioavailability. *Environ Sci Technol* **1997**, *31*, 248–252.
- 545 [45] Ehrl, B.; Gharasoo, M.; Elsner, M. Isotope Fractionation Pinpoints Membrane Permeability as a Barrier to Atrazine
546 Biodegradation in Gram-negative Polaromonas sp. Nea-C. *Environ Sci Technol* **2018**, *52*, 4137–4144.
- 547 [46] Gharasoo, M.; Ehrl, B. N.; Cirpka, O. A.; Elsner, M. Modeling of Contaminant Biodegradation and Compound-Specific
548 Isotope Fractionation in Chemostats at Low Dilution Rates. *Environ Sci Technol* **2019**, *53*, 1186–96.
- 549 [47] Hesse, F.; Harms, H.; Attinger, S.; Thullner, M. Linear Exchange Model for the Description of Mass Transfer Limited
550 Bioavailability at the Pore Scale. *Environ Sci Technol* **2010**, *44* (6), 2064–2071.
- 551 [48] Ramsay, R.; Tipton, K. Assessment of Enzyme Inhibition: A Review with Examples from the Development of
552 Monoamine Oxidase and Cholinesterase Inhibitory Drugs. *Molecules* **2017**, *22*(7), 1192.
- 553 [49] Haws, N. W.; Ball, W. P.; Bouwer, E. J. Modeling and interpreting bioavailability of organic contaminant mixtures in
554 subsurface environments. *J Contam Hydrol* **2006**, *82*, 255–292.
- 555 [50] Lehninger, A. L.; Nelson, D. L.; Cox, M. M. *Lehninger Principles of Biochemistry*; W. H. Freeman, 2005.
- 556 [51] Thullner, M.; Regnier, P.; Van Cappellen, P. Modeling Microbially Induced Carbon Degradation in Redox-Stratified
557 Subsurface Environments: Concepts and Open Questions. *Geomicrobiol J* **2007**, *24*, 139–155.
- 558 [52] Nowak, W.; Schwede, R. L.; Cirpka, O. A.; Neuweiler, I. Probability density functions of hydraulic head and velocity
559 in three-dimensional heterogeneous porous media. *Water Resour Res* **2008**, *44*.
- 560 [53] Dietrich, C. R.; Newsam, G. N. A fast and exact method for multidimensional gaussian stochastic simulations. *Water*
561 *Resour Res* **1993**, *29*, 2861–2869.
- 562 [54] Gharasoo, M.; Centler, F.; Fetzer, I.; Thullner, M. How the chemotactic characteristics of bacteria can determine their
563 population patterns. *Soil Biol Biochem* **2014**, *69*, 346–358.
- 564 [55] Lopez-Peña, L. A.; Meulenbroek, B.; Vermolen, F. A network model for the biofilm growth in porous media and its
565 effects on permeability and porosity. *Comput Visual Sci* **2019**, *21*, 11–22.
- 566 [56] Harms, H.; Zehnder, A. J. Influence of substrate diffusion on degradation of Dibenzofuran and 3-Chlorodibenzofuran
567 by attached and suspended bacteria. *Appl Environ Microbiol* **1994**, *60*, 2736–2745.
- 568 [57] Jung, H.; Meile, C. Upscaling of microbially driven first-order reactions in heterogeneous porous media. *J Contam*
569 *Hydrol* **2019**, *224*, 103483.
- 570 [58] Gharasoo, M.; Thullner, M.; Elsner, M. Introduction of a new platform for parameter estimation of kinetically complex
571 environmental systems. *Environ Model Softw* **2017**, *98*, 12–20.
- 572 [59] Regnier, P.; O’Kane, J.; Steefel, C.; Vanderborcht, J. Modeling complex multi-component reactive-transport systems:
573 towards a simulation environment based on the concept of a Knowledge Base. *Appl Math Model* **2002**, *26*, 913–927.
- 574 [60] Sun, X.; Duddu, R. A sequential non-iterative approach for modeling multi-ionic species reactive transport during
575 localized corrosion. *Finite Elem Anal Des* **2019**, *166*, 103318.
- 576 [61] Liu, X.; Gharasoo, M.; Shi, Y.; Sigmund, G.; Hüffer, T.; Duan, L.; Wang, Y.; Ji, R.; Hofmann, T.; Chen, W. *Environ*
577 *Sci Technol* **2020**, *54*, 12051–62.
- 578 [62] Sobol, I. Global sensitivity indices for nonlinear mathematical models and their Monte Carlo estimates. *Math Comput*
579 *Simul* **2001**, *55*, 271–280.
- 580 [63] Kampara, M.; Thullner, M.; Richnow, H. H.; Harms, H.; Wick, L. Y. Impact of Bioavailability Restrictions on Micro-
581 bially Induced Stable Isotope Fractionation. 2. Experimental Evidence. *Environ Sci Technol* **2008**, *42*, 6552–58.
- 582 [64] Marozava, S.; Meyer, A. H.; Pérez-de Mora, A.; Gharasoo, M.; Zhuo, L.; Wang, H.; Cirpka, O. A.; Meckenstock, R. U.;
583 Elsner, M. Mass Transfer Limitation during Slow Anaerobic Biodegradation of 2-Methylnaphthalene. *Environ Sci*
584 *Technol* **2019**, *53*, 9481–9490.
- 585 [65] Thullner, M.; Kampara, M.; Richnow, H. H.; Harms, H.; Wick, L. Y. Impact of Bioavailability Restrictions on Micro-
586 bially Induced Stable Isotope Fractionation. 1. Theoretical Calculation. *Environ Sci Technol* **2008**, *42*, 6544–51.

	Michaelis-Menten Eq. (2)	Mass-transfer Best Eq. (4)	Self-inhibition Haldane Eq. (6)	Bioavailability + Self-inhibition Eq. (7)
Homogeneous	0.0594	0.1004	1.1007	1.0943
Heterogeneous stdv = 45 μ m lx=1mm	0.0713 \pm 0.0007	0.1194 \pm 0.0005	1.0985 \pm 0.0001	1.0904 \pm 0.0001
Heterogeneous stdv = 45 μ m lx=2.5mm	0.0899 \pm 0.0072	0.1368 \pm 0.0068	1.0968 \pm 0.0006	1.0887 \pm 0.0006
Heterogeneous stdv = 45 μ m lx=5mm	0.1085 \pm 0.0134	0.1556 \pm 0.01201	1.0946 \pm 0.0009	1.0865 \pm 0.0009
Heterogeneous stdv = 70 μ m lx=1mm	0.0923 \pm 0.0056	0.1516 \pm 0.0051	1.0968 \pm 0.0003	1.0854 \pm 0.0006
Heterogeneous stdv = 70 μ m lx=2.5mm	0.1272 \pm 0.0252	0.1843 \pm 0.0212	1.0925 \pm 0.0037	1.0809 \pm 0.0050
Heterogeneous stdv = 70 μ m lx=5mm	0.1694 \pm 0.0581	0.2241 \pm 0.0523	1.0866 \pm 0.0093	1.0744 \pm 0.0129

Table 1: Average outlet concentrations (μ M) from pore network simulations for each scenario at steady state, and for different kinetics of substrate degradation. The standard errors are calculated from the five corresponding realizations for each scenario. Note that the inlet concentration was fixed at 1.55 μ M in all the scenarios. Normalized results in respect to the inlet concentration and the homogeneous case are summarized, illustrated, and compared in Fig. 5. stdv = standard deviation, lx = correlation length.

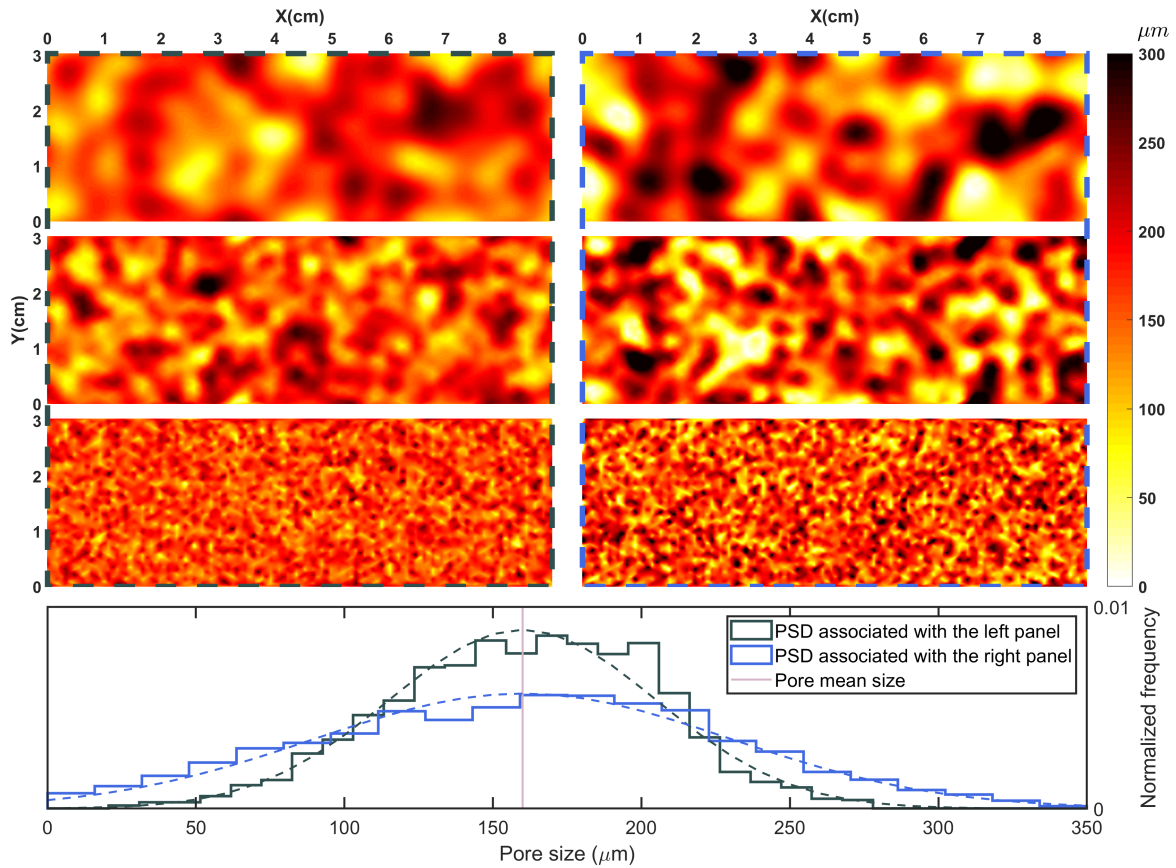


Figure 1: Pore size (radius) distributions in heterogeneous pore networks. A random realization of each scenario (except the homogeneous one) is shown. Pore-scale heterogeneities were generated with a mean pore-size of $160\mu m$ and a standard deviation of $45\mu m$ (Top-Left panel) and $70\mu m$ (Top-Right panel). In both panels, the correlation length decrease from top to bottom (5, 2.5 and 1 mm, respectively). The pore size histograms associated with the two normal distributions of the radii are shown at bottom. Dashed lines are the probability (or Gaussian) density functions associated with the two histograms.

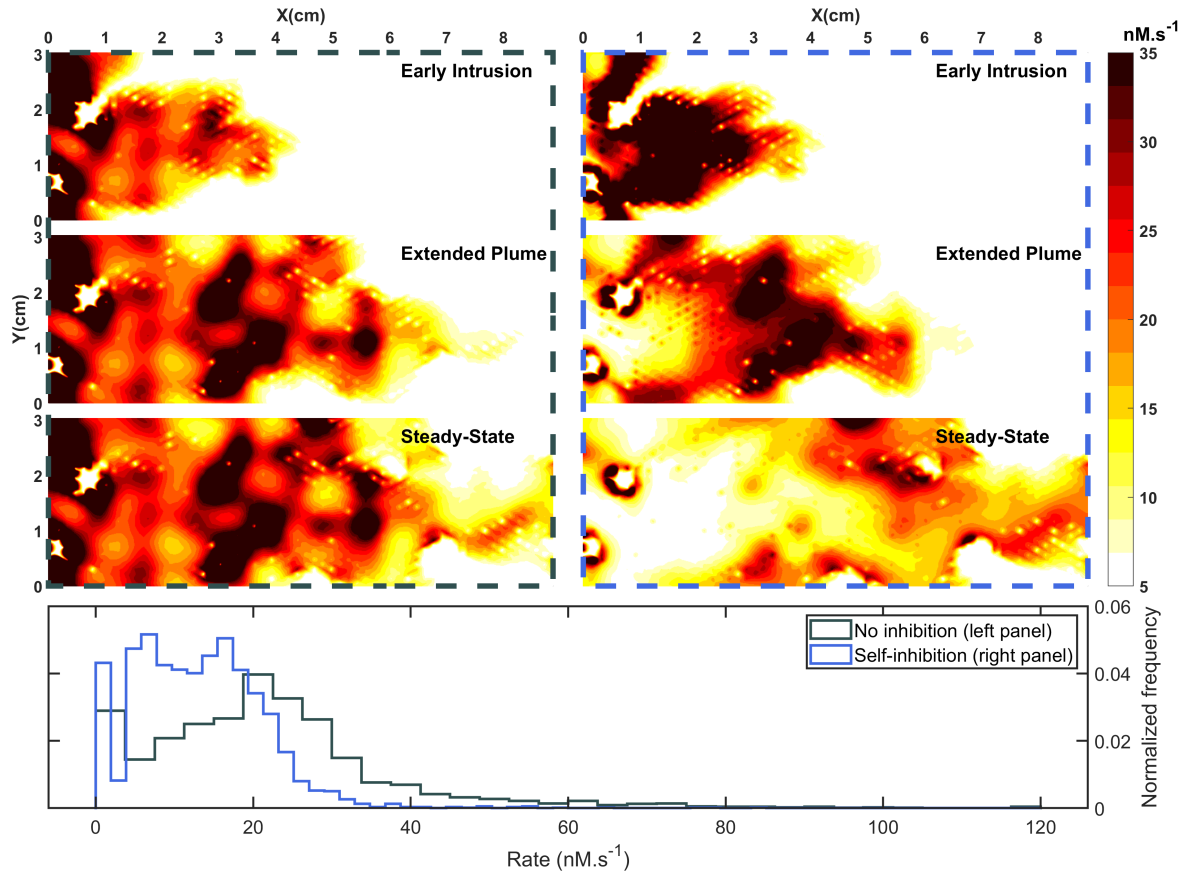


Figure 2: Spatial and temporal distribution of rates in a heterogeneous medium. The expansion of the contaminant plume inside one of the heterogeneous scenarios (pore-size stdv of $70\mu\text{m}$ and the correlation length of 5mm shown in Fig. 1 top-right) at different times in the absence (Left panel) and the presence of self-inhibition (Right panel). The histogram of distribution of the rates at steady-state is shown for both cases (Bottom).

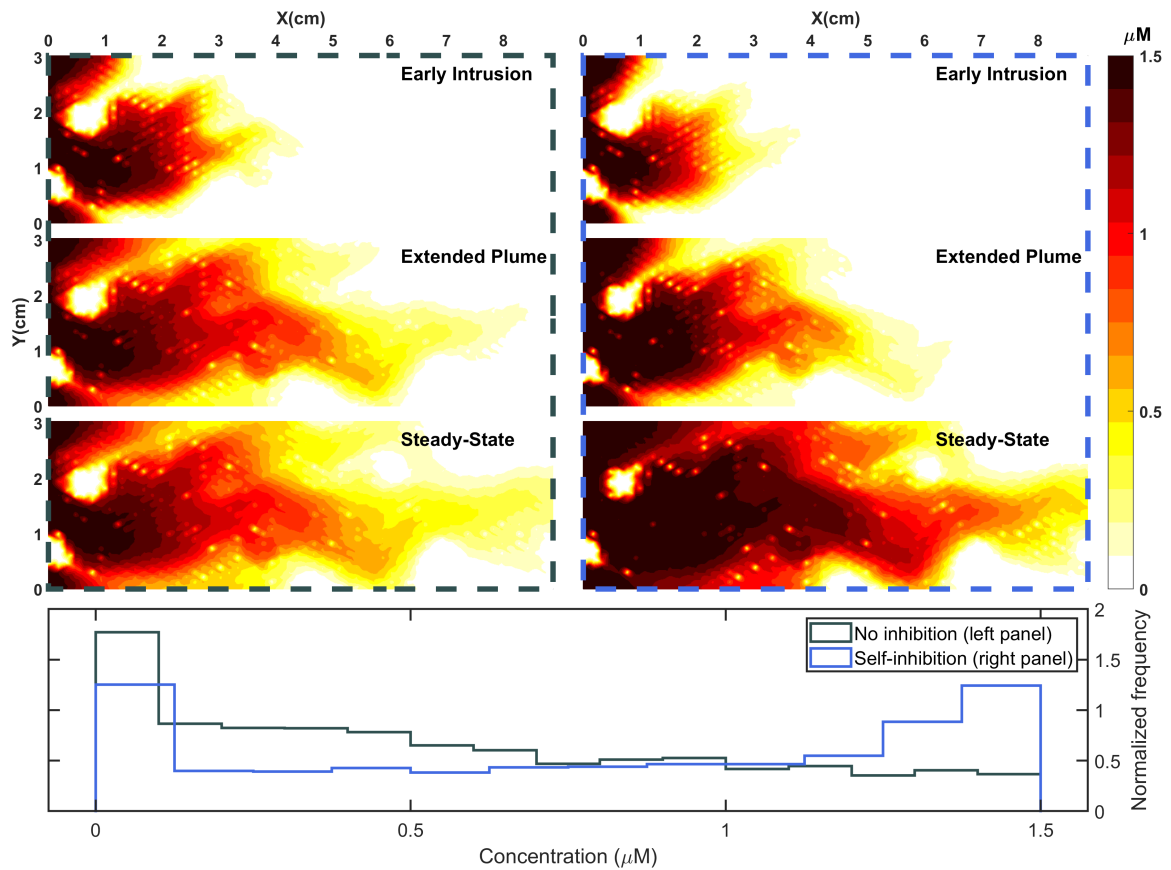


Figure 3: Spatial and temporal distribution of concentrations in a heterogeneous medium. The expansion of the contaminant plume inside the same heterogeneous scenario as in Fig. 2 is shown at different times in the absence (Left panel) and the presence of self-inhibition (Right panel). The histogram of pore concentrations at steady-state is shown for both cases (Bottom).

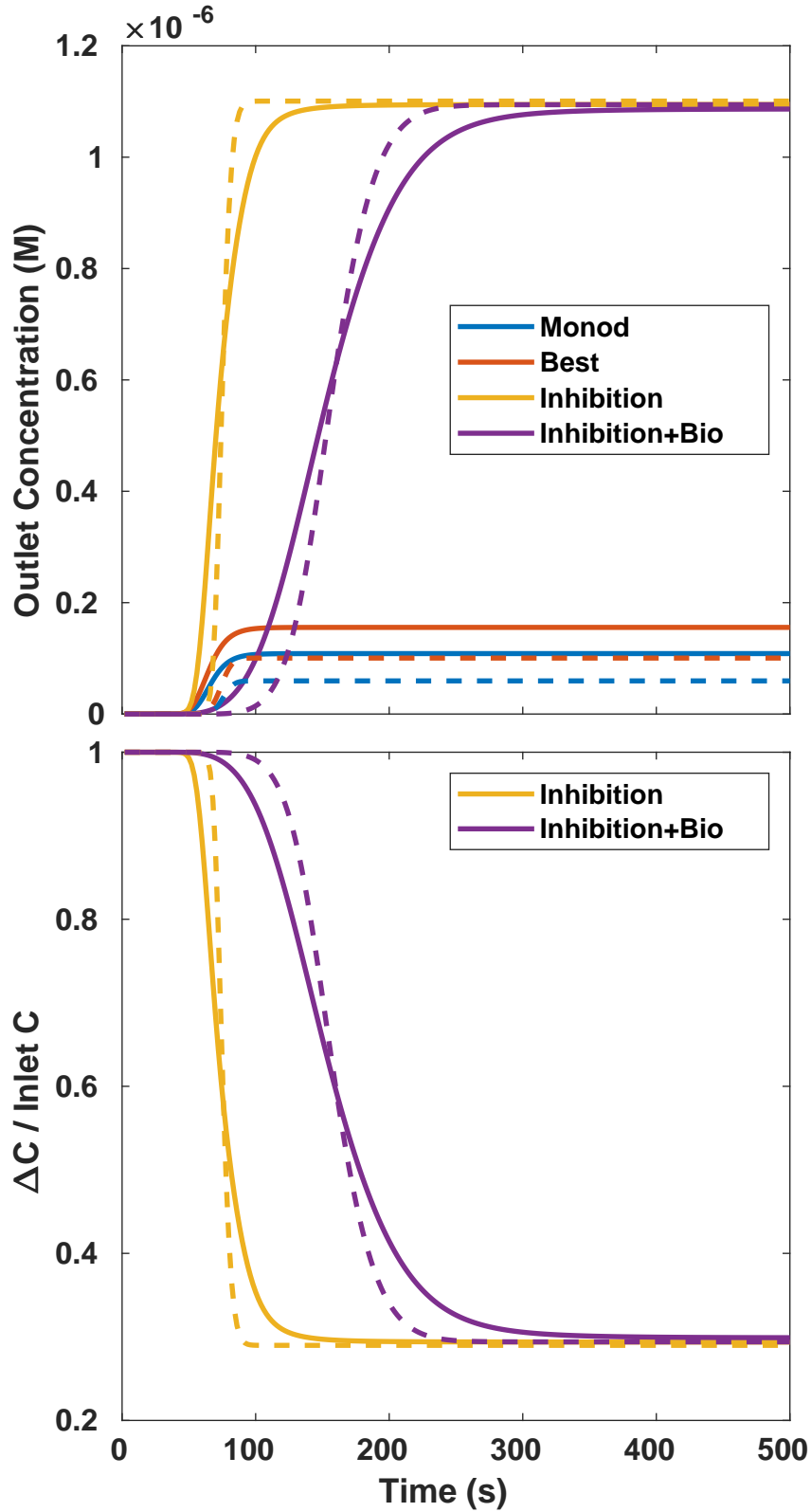


Figure 4: The transient and steady-state outlet concentrations and dimensionless medium degradation capacity ($\Delta C = \frac{C_{out} - C_{in}}{C_{in}}$) compared between the homogeneous pore network scenario (dashed lines) and a heterogeneous pore network scenario (solid lines) with pore size stdv = $70\mu\text{m}$ and correlation length of 5mm (a realization from this scenario is shown in Fig. 1: Top-Right).

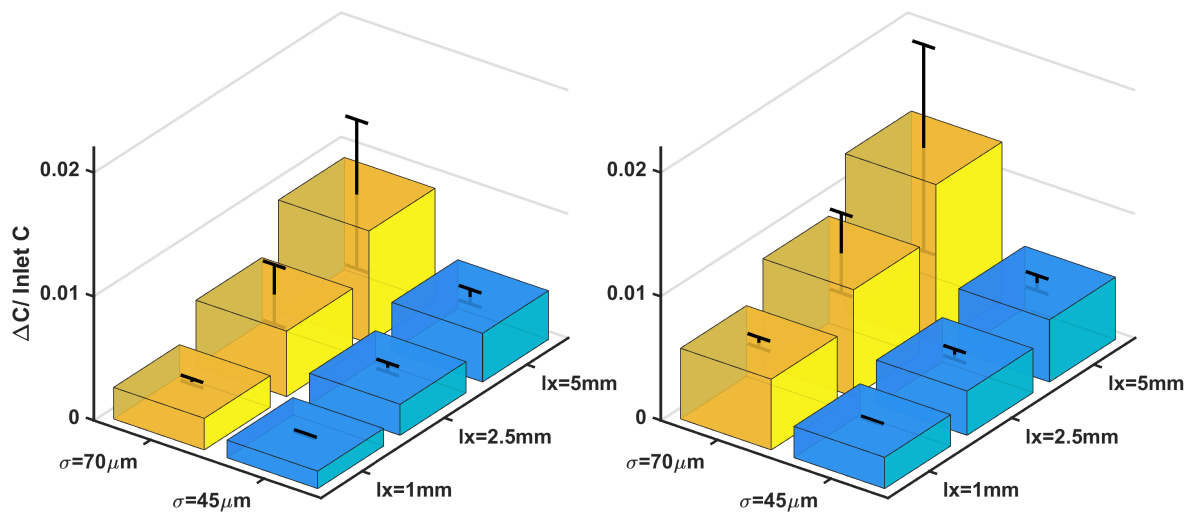


Figure 5: Comparison between overall steady-state degradation in pore networks with various pore-size heterogeneities and in reference to the homogeneous case scenario (at level zero). Left: The results when only non-competitive inhibition was considered Eq. (6). Right: When both inhibition and small-scale bioavailability limitations are present Eq. (7). The numeric values for this chart are listed in Table 1. The error bars show the standard deviations calculated for each scenario from their respective five realizations. The six different heterogeneous scenarios were made by combining three spatial correlation lengths (l_x) and two pore-size standard deviations (σ).